

Article

# Effect of T6 Heat Treatment on Microstructure and Hardness of Nanosized Al<sub>2</sub>O<sub>3</sub> Reinforced 7075 Aluminum Matrix Composites

Peng-Xiang Zhang <sup>1</sup>, Hong Yan <sup>1,\*</sup> , Wei Liu <sup>1</sup>, Xiu-Liang Zou <sup>1</sup> and Bin-Bing Tang <sup>2</sup>

<sup>1</sup> School of Mechanical and Electrical Engineering, Nanchang University, Nanchang 330031, China; pxzhang1021@163.com (P.-X.Z.); chentailiu@outlook.com (W.L.); xiuliangzou@yeah.net (X.-L.Z.)

<sup>2</sup> Institute for Advanced Study, Nanchang University, Nanchang 330031, China; binbingtang@ncu.edu.cn

\* Correspondence: yanhong\_wh@163.com; Tel.: +86-791-8396-9633; Fax: +86-791-8396-9622

Received: 6 December 2018; Accepted: 1 January 2019; Published: 5 January 2019



**Abstract:** In this study, 7075 aluminum matrix composites reinforced with 1.5 wt.% nanosized Al<sub>2</sub>O<sub>3</sub> were fabricated by ultrasonic vibration. The effect of T6 heat treatment on both microstructure and hardness of nanosized Al<sub>2</sub>O<sub>3</sub> reinforced 7075 (Al<sub>2</sub>O<sub>3np</sub>/7075) composites were studied via scanning electron microscopy, energy dispersive X-ray spectrometry, X-ray diffraction, transmission electron microscopy, and hardness tests. The Mg(Zn,Cu,Al)<sub>2</sub> phases gradually dissolved into the matrix under solution treatment at 480 °C for 5 h. However, the morphology and size of Al<sub>7</sub>Cu<sub>2</sub>Fe phases remained unchanged due to their high melting points. Furthermore, the slenderness strips MgZn<sub>2</sub> phases precipitated under aging treatment at 120 °C for 24 h. Compared to as-cast composites, the hardness of the sample under T6 heat treatment was increased ~52%. The strengthening mechanisms underlying the achieved hardness of composites are revealed.

**Keywords:** Al<sub>2</sub>O<sub>3np</sub>/7075 composites; T6 heat treatment; microstructure; hardness; strengthening mechanism

## 1. Introduction

Aluminum alloy matrix composites are widely used in the automobile and communication industries, as well as in military and aerospace series due to their high specific strengths, specific stiffnesses, specific moduli, and low coefficients of linear expansion properties [1]. Aluminum alloy matrix composites have recently developed into high-profile emerging materials [2,3].

To improve the mechanical properties and optimize the microstructure of aluminum alloy, micro-sized ceramic reinforced particles were added into aluminum alloy matrixes by metal matrix composites (MMCs) [4–6]. However, the achieved improvement of mechanical properties of micro-sized ceramic particles reinforced composites is limited [7–9], while nanosized ceramic reinforced particles can greatly improve the tensile strength, yield strength, and hardness of the composites [10,11]. Besides the size of ceramic reinforced particles, the microstructure and mechanical properties of particles reinforced aluminum alloy matrix composites are affected by many other factors, including the volume fraction of the ceramic reinforced particles, the composition of the aluminum alloy matrix, the grain size, the heat treatment technology and so on [12].

Of all the factors listed, heat treatment plays an important role in improving the microstructure and overall properties of composites. Li et al. [13] reported that the eutectic Si led to spheroidization during the solution treatment, and the needle-like Al<sub>2</sub>Cu phases precipitated after aging treatment. The hardness of SiC<sub>p</sub>/Al-5Si-1Cu-0.5Mg aluminum matrix composites increased by 17%. The friction coefficient and the wear rate of composites decreased greatly compared with as-cast composites.

Lashgari et al. [14] found that eutectic silicon of A356-10%B<sub>4</sub>C aluminum matrix composites changed from acicular to spheroidized after heat treatment, and the yield stress and wear resistance of composites were increased by performing heat treatment. Albiter et al. [15] reported that the large amount of CuAl<sub>2</sub> phase in the Al-2024/TiC composites precipitated and became more dispersed after heat treatment. The hardness and the ultimate tensile strength of 55% TiC composites increased from 28.5 to 38.5 HRC and from 379 to 480 MPa, respectively. In a word, the use of appropriate heat treatment technology can improve the microstructure and hardness of composites.

In previous research works, 7075 aluminium matrix composites reinforced with 1.5 wt.% Al<sub>2</sub>O<sub>3np</sub> were fabricated by ultrasonic vibration. Meanwhile, the microstructure, ultimate tensile strength and 0.2 compressive yield strength of the Al<sub>2</sub>O<sub>3np</sub>/7075 composites were analyzed [16]. However, research on the effects of heat treatment on nano-ceramic particle reinforced aluminum matrix composites is currently missing. This study evaluates the effects of T6 heat treatment on the microstructure and hardness of 1.5 wt.% Al<sub>2</sub>O<sub>3np</sub>/7075 composites and reveals the strengthening mechanism of composites. The obtained results provide guiding implications for the preparation of nanosized reinforced particle aluminum matrix composites.

## 2. Experiment

The matrix materials employed for the preparation of composites were commercial 7075 aluminum alloy. Its chemical composition is shown in Table 1. The materials utilized in this experiment were prepared by casting. In the casting process of composites, Mg powders with a purity of 99.9% and average particle size is 58–75 μm were used as the wetting agent, and nanosized α-Al<sub>2</sub>O<sub>3</sub> powders with a purity of 99.9% and average particle diameter of 80 nm were used as reinforcement.

**Table 1.** Chemical composition of 7075 aluminum alloy (mass fraction, %).

Zn	Mg	Cu	Mn	Cr	Si	Fe	Ti	Al
5.23	2.10	1.45	0.30	0.23	0.22	0.22	0.16	Balance

The Al<sub>2</sub>O<sub>3np</sub>-containing Mg powder was prepared by ball milling on a planetary ball milling machine(WXQM-4, TENCAN POWDER Co., Ltd., Changsha, China) at a constant rotation speed of 100 rpm for 30 min. The method has been thoroughly described in [17]. The 7075 aluminum matrix was melted in a clay-graphite crucible inside a resistance furnace under a protective argon gas atmosphere at 800 °C. The clay-graphite crucible is 50 mm in inner diameter and 60 mm in height. The powder was wrapped in aluminum foils and divided into equal portions, and the quality of each portions powder is 0.3 g. A portion powder was added to the melt for every minute. With the addition of powder, the melt was subjected to ultrasonic vibration at a power level of 1000 W and a frequency of 10 kHz. The diameter of the probe tip is 20 mm. After the completion of powder addition, the melt was subjected to ultrasonic vibration at a power level of 1000 W and a frequency of 20 kHz for 10 min. The different ultrasonic frequencies were used in the different steps in order to the Al<sub>2</sub>O<sub>3np</sub> particles were distributed and dispersed uniformly in the melt. The composites slurries were cast into a steel mold.

Composite ingots containing 1.5 wt.% Al<sub>2</sub>O<sub>3np</sub> were processed into small samples of Φ10 mm × 10 mm. The T6 heat treatment processes were conducted in a box-type with temperature control resistance furnace (SX24-13, Shanghai Y-Feng Electrical Furnace Co., Ltd., Shanghai, China), the heat treatment process scheme is presented in Table 2.

**Table 2.** The heat treatment processes scheme.

No.	Heat Treatment Processes Scheme
1	(480 °C, 5 h) + water quench (25 ± 5 °C)
2	(480 °C, 5 h) + water quench (25 ± 5 °C) + (120 °C, 8 h)
3	(480 °C, 5 h) + water quench (25 ± 5 °C) + (120 °C, 16 h)
4	(480 °C, 5 h) + water quench (25 ± 5 °C) + (120 °C, 24 h)
5	(480 °C, 5 h) + water quench (25 ± 5 °C) + (120 °C, 32 h)
6	(480 °C, 5 h) + water quench (25 ± 5 °C) + (80 °C, 24 h)
7	(480 °C, 5 h) + water quench (25 ± 5 °C) + (100 °C, 24 h)
8	(480 °C, 5 h) + water quench (25 ± 5 °C) + (140 °C, 24 h)

The microstructure of the composites was observed via scanning electron microscopy (SEM, Tescan-Vega3, TESCAN CHINA Co., Ltd., Shanghai, China) equipped with energy dispersive X-ray spectrometry (EDS, TESCAN CHINA, Co., Ltd., Shanghai, China). Prior to scanning electron examinations, the samples were ground, polished, etched with 0.5% (volume fraction) hydrofluoric acid for up to 5 s, and then rinsed with distilled water. To ensure the accuracy of the stoichiometries and the qualitative determination of phases, at least six EDS random measurements were conducted for each phase. The transformation of phases under different heat treatment was obtained via X-ray diffraction (XRD, D8 ADVANCE, Bruker Beijing Scientific Technology Co., Ltd., Beijing, China). Transmission electron microscopy (TEM, JEM-2100, Japan Electronics Co., Ltd., Tokyo, Japan) was used to verify the existence and microstructure of the specific phase. Prior to TEM, the samples of  $\Phi 3 \text{ mm} \times 0.1 \text{ mm}$  were thinned to dozens of nanometer thickness via electrolytic dual spray reduction instrument (MTP-1A, JIAODA Co., Ltd., Shanghai, China) and precision ion polishing system (Fischione-100, E.A. Fischione Instruments, Inc., Murrysville, PA, USA). The Vickers hardness of composites samples were obtained via hardness tester device (HV 1000 A, Laizhou Huayin Testing Instrument Co., Ltd., Laizhou, China). To ensure the accuracy of the data, at least seven random hardness measurements were conducted for each sample.

### 3. Results and Discussion

#### 3.1. Microstructure Evolution

The microstructure of the 7075 aluminum matrix as-cast is shown in Figure 1a. It can be concluded that the microstructure of 7075 aluminum matrix as-cast consists mainly of  $\alpha$ -Al and dendritic eutectic phase. Figure 1b shows the microstructure of the  $\text{Al}_2\text{O}_{3\text{np}}/7075$  composites. The  $\alpha$ -Al phases were significantly refined, and the eutectic phases were more uniform and dispersed. When the  $\text{Al}_2\text{O}_{3\text{np}}/7075$  composites had been solution treatment at 480 °C for 5 h, the eutectic phases were interrupted and discontinuous. It can be observed that most of eutectic phases were dissolved in the matrix, and a few insoluble phases remained, as shown in Figure 1c. After aging treatment, a large number of eutectic phases were precipitated. However, because the size of precipitated phases is extremely small, there is no significant difference between the microstructure of the  $\text{Al}_2\text{O}_{3\text{np}}/7075$  composites under solution treatment and the microstructure of the  $\text{Al}_2\text{O}_{3\text{np}}/7075$  composites under aging treatment with different temperature and time. The microstructure of  $\text{Al}_2\text{O}_{3\text{np}}/7075$  composites under solution treatment at 480 °C for 5 h and aging treatment at 120 °C for 24 h is shown in Figure 1d, and the microstructure of the precipitated phase was observed by TEM.

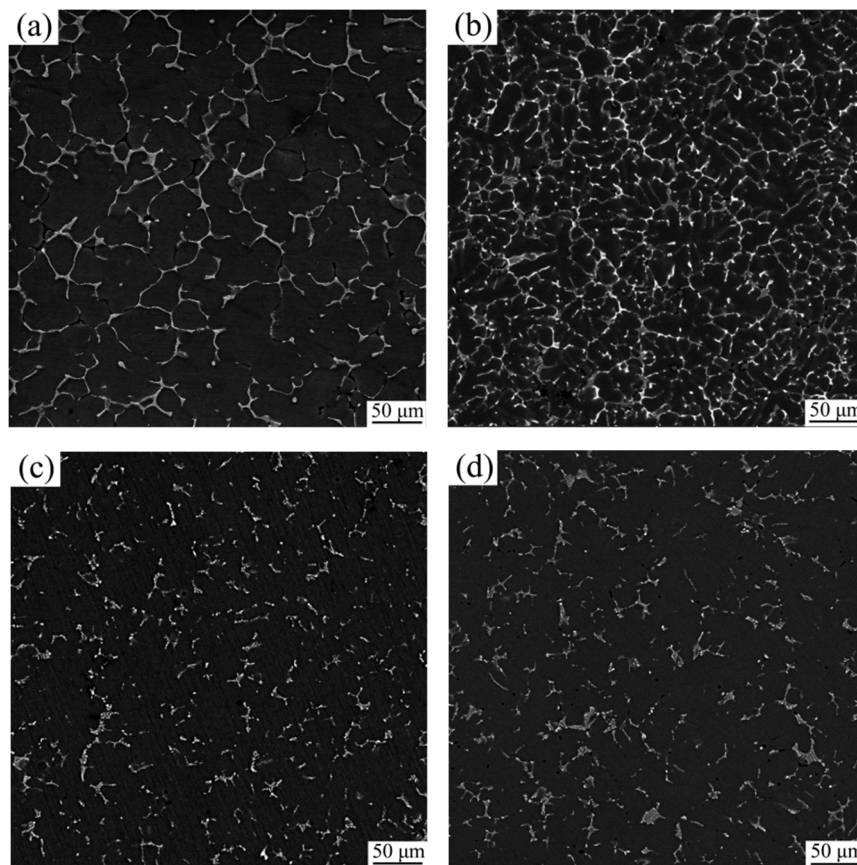


**Figure 1.** The microstructure of: (a) 7075 aluminum matrix as-cast; (b)  $\text{Al}_2\text{O}_{3\text{np}}/7075$  composites; (c)  $\text{Al}_2\text{O}_{3\text{np}}/7075$  composites under solution treatment at  $480\text{ }^\circ\text{C}$  for 5 h; (d)  $\text{Al}_2\text{O}_{3\text{np}}/7075$  composites under solution treatment at  $480\text{ }^\circ\text{C}$  for 5 h and aging treatment at  $120\text{ }^\circ\text{C}$  for 24 h.

The microstructure and EDS spectra of eutectic phases of  $\text{Al}_2\text{O}_{3\text{np}}/7075$  composites are shown in Figure 2a–c, respectively. It can be observed that the eutectic phases of  $\text{Al}_2\text{O}_{3\text{np}}/7075$  composites were mainly composed of lamellar structures and massive structures. The EDS analysis result shows that the stoichiometries of the lamellar eutectic phase are 81.13% Al, 7.08% Zn, 3.79% Mg, and 7.99% Cu (molar fraction), as shown in Figure 2b, which are similar to the stoichiometries of  $\text{Mg}(\text{Zn,Cu,Al})_2$  phases. The EDS analysis result indicates that the stoichiometries of the massive eutectic phase are 78.98% Al, 1.98% Zn, 2.43% Mg, 11.19% Cu, and 5.42% Fe (molar fraction), as shown in Figure 2c, which are similar to the stoichiometries of  $\text{Al}_7\text{Cu}_2\text{Fe}$  phases [18].

Figure 2d–f show the microstructure and EDS spectra of  $\text{Al}_2\text{O}_{3\text{np}}/7075$  composites at high magnification obtained under solution treatment at  $480\text{ }^\circ\text{C}$  for 5 h, respectively. The morphology and size of the massive  $\text{Al}_7\text{Cu}_2\text{Fe}$  phases show no change during the solution treatment due to its high melting point, and the EDS analysis result of  $\text{Al}_7\text{Cu}_2\text{Fe}$  phases is shown in Figure 2f. The lamellar eutectic  $\text{Mg}(\text{Zn,Cu,Al})_2$  phases almost completely disappeared. Meanwhile, a new eutectic phase formed. The EDS analysis result shows that the stoichiometries of the new phase are 80.60% Al, 4.06% Zn, 7.24% Mg, and 8.11% Cu (molar fraction), as shown in Figure 2e, which are similar to the stoichiometries of the  $\text{Al}_2\text{CuMg}$  phases, and the reason for the formation of  $\text{Al}_2\text{CuMg}$  phases is that the diffusion velocity of Cu is slower than that of Zn and Mg [19].

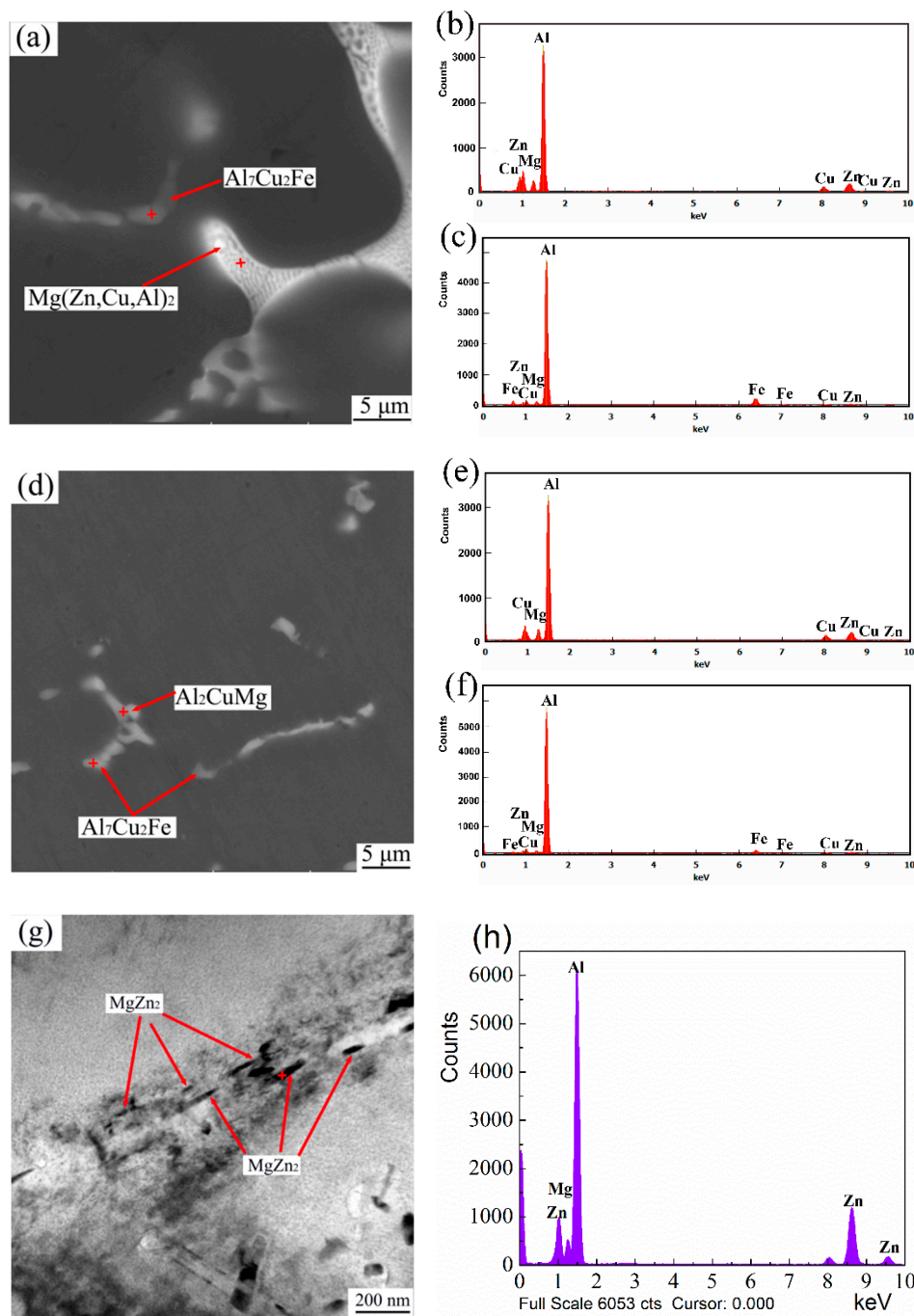


**Figure 2.** (a) The microstructure of eutectic phases of Al<sub>2</sub>O<sub>3</sub>np/7075 composites; (b) The EDS spectra results of the Mg(Zn,Cu,Al)<sub>2</sub> phases; (c) The EDS spectra results of Al<sub>7</sub>Cu<sub>2</sub>Fe phases; (d) The microstructure of eutectic phases of Al<sub>2</sub>O<sub>3</sub>np/7075 composites under solution treatment at 480 °C for 5 h; (e) The EDS spectra results of Al<sub>2</sub>CuMg phases; (f) The EDS spectra results of Al<sub>7</sub>Cu<sub>2</sub>Fe phases; (g) The TEM of precipitated phases of Al<sub>2</sub>O<sub>3</sub>np/7075 composites under T6 heat treatment at 480 °C for 5 h and 120 °C for 24 h; (h) The EDS spectra results of MgZn<sub>2</sub> phases.

The TEM and EDS of precipitated phases of Al<sub>2</sub>O<sub>3</sub>np/7075 composites under T6 heat treatment at 480 °C for 5 h and 120 °C for 24 h is shown in Figure 2g,h, respectively. It can be observed that the aging precipitated phases were clubbed, small, and grow along grain boundaries. The EDS analysis result shows that the ratio of Mg to Zn is almost 1:2, which is similar to the stoichiometries of MgZn<sub>2</sub> phases.

The XRD patterns of the  $\text{Al}_2\text{O}_{3\text{np}}/7075$  composites under different heat treatment condition are shown in Figure 3. The dominant second phase in the solidification eutectic should be the  $\text{MgZn}_2$  phase, as indicated by previous investigations [20]. The  $\text{Mg}(\text{Zn,Cu,Al})_2$  eutectic phases can be formed because the Al and Cu atoms have dissolved into the  $\text{MgZn}_2$  phases, and the crystallographic lattice constant of  $\text{Mg}(\text{Zn,Cu,Al})_2$  phases is similar to  $\text{MgZn}_2$  phases [21]. The  $\text{MgZn}_2$  phase peak can be found in the XRD patterns of the as-cast  $\text{Al}_2\text{O}_{3\text{np}}/7075$  composites. After solution treatment at  $480^\circ\text{C}$  for 5 h, the  $\text{Mg}(\text{Zn,Cu,Al})_2$  phases almost completely disappeared, and the  $\text{Al}_2\text{CuMg}$  phases formed. The  $\text{Al}_2\text{CuMg}$  phases peak can be found in the XRD patterns of the  $\text{Al}_2\text{O}_{3\text{np}}/7075$  composites under heat treatment at  $480^\circ\text{C}$  for 5 h. After solution treatment at  $480^\circ\text{C}$  for 5 h and aging treatment at  $120^\circ\text{C}$  for 24 h, the  $\text{MgZn}_2$  phases precipitated. The  $\text{MgZn}_2$  phases peak can be found in the XRD patterns of the  $\text{Al}_2\text{O}_{3\text{np}}/7075$  composites under heat treatment at  $480^\circ\text{C}$  for 5 h and  $120^\circ\text{C}$  for 24 h. The  $\text{Al}_7\text{Cu}_2\text{Fe}$  phases peak always exists in the XRD patterns, and the  $\text{Al}_7\text{Cu}_2\text{Fe}$  phases show almost no change under different processing states, which is consistent with the result of XRD.

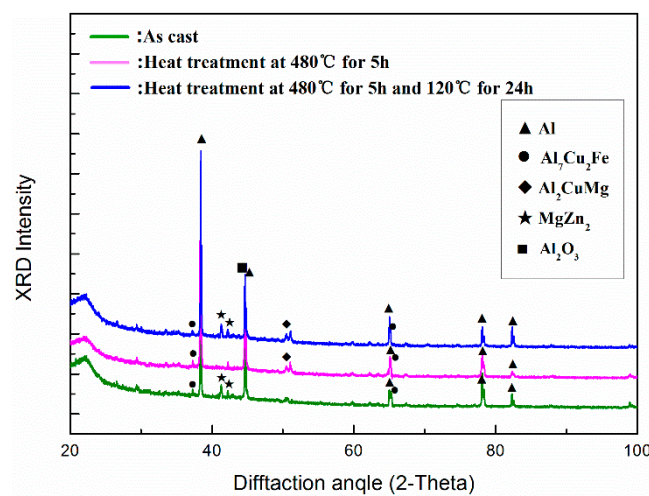


**Figure 3.** XRD patterns of the  $\text{Al}_2\text{O}_{3\text{np}}/7075$  composites under different heat treatment condition.

### 3.2. Strengthening Mechanism and Hardness

The distribution schematic of the  $\text{Al}_2\text{O}_{3\text{np}}$  reinforced particles in 7075 aluminum under different processing states are shown in Figure 4. These  $\text{Al}_2\text{O}_{3\text{np}}$  particles were distributed and dispersed uniformly in the melt. Single  $\text{Al}_2\text{O}_{3\text{np}}$  particles, small aggregates of  $\text{Al}_2\text{O}_{3\text{np}}$  particles and large aggregates of  $\text{Al}_2\text{O}_{3\text{np}}$  particles were distributed inside the grains, and medium sized aggregates of  $\text{Al}_2\text{O}_{3\text{np}}$  particles ranging were located in the grain boundary, as Schultz et al. [22] reported. The  $\text{Al}_2\text{O}_{3\text{np}}$  particles aggregates dispersed eutectic phase, and the pinning effect of medium sized aggregates prevented grain growth. And the distributed  $\text{Al}_2\text{O}_{3\text{np}}$  particles inhibited the trend of grain growth during heat treatment process.

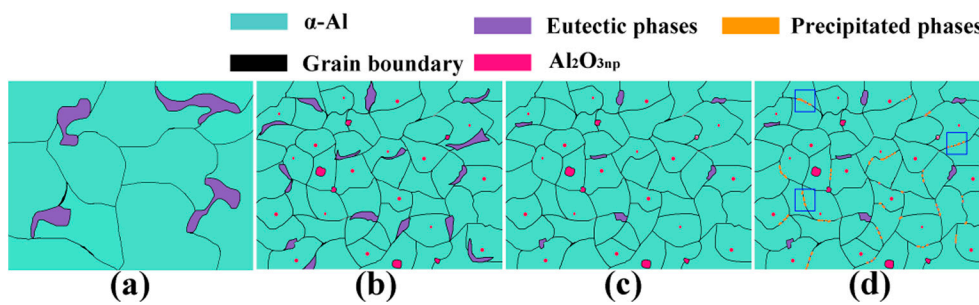


**Figure 4.** The distribution schematic of  $\text{Al}_2\text{O}_{3\text{np}}$  reinforced particles in 7075 aluminum under different processing states: (a) 7075 aluminum matrix as-cast; (b)  $\text{Al}_2\text{O}_{3\text{np}}$ /7075 composites; (c)  $\text{Al}_2\text{O}_{3\text{np}}$ /7075 composites under heat treatment at 480 °C for 5 h; (d)  $\text{Al}_2\text{O}_{3\text{np}}$ /7075 composites under heat treatment at 480 °C for 5 h and 120 °C for 24 h.

Figure 5 shows the hardness of both 7075 aluminum matrix and  $\text{Al}_2\text{O}_{3\text{np}}$ /7075 composites as a result of different heat treatments. Compared to the hardness of 7075 aluminum matrix (94.7 HV), the hardness of  $\text{Al}_2\text{O}_{3\text{np}}$ /7075 composites (113.8 HV) increased ~20%. There is a close crystal structure between  $\text{Al}_2\text{O}_3$  and  $\alpha\text{-Al}$  [23]. Thus,  $\text{Al}_2\text{O}_{3\text{np}}$  particles are able to serve as the substrates for heterogeneous nucleation, which indicates that the composites form a larger number of grains than the matrix. According to the Hall-Petch formula [24]:

$$\sigma_y = \sigma_0 + k_y d^{-1/2}, \quad (1)$$

where  $\sigma_y$  represents the yield strength;  $\sigma_0$  and  $k_y$  represent the constants about the material;  $d$  represents the average diameter of grain. The strength of the composites is inversely proportional to the average diameter of the grain. Finer the grain size leads to higher strength of the composite. There is a positive correlation between strength and hardness of the composite. Generally speaking, the higher the strength of composite, the higher the hardness.

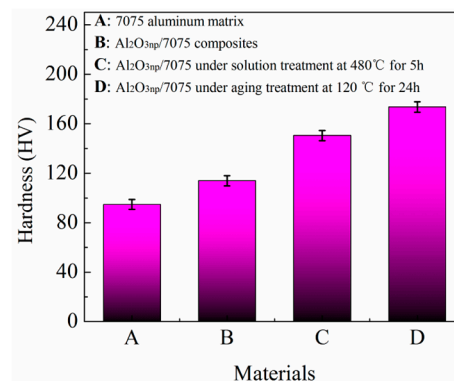


**Figure 5.** The hardness of 7075 aluminum matrix and  $\text{Al}_2\text{O}_{3\text{np}}$ /7075 composites under different heat treatment.

In addition,  $\text{Al}_2\text{O}_3$  form a coherent or semi-coherent interface with  $\alpha\text{-Al}$ , but lattice constant contains deviations which lead to the occurrence of lattice distortion. The interaction of lattice distortion stress field and dislocation stress field becomes stronger, and the hindrance effect of dislocation motion is increased. Meanwhile, according to the Orowan strengthening mechanism, the dislocation lines bypass the  $\text{Al}_2\text{O}_{3\text{np}}$  particles when the dislocation lines move near the  $\text{Al}_2\text{O}_{3\text{np}}$  particles; furthermore, dislocation rings form around the  $\text{Al}_2\text{O}_{3\text{np}}$  particles. The schematic illustration of dislocation lines through the particle mechanism is shown in Figure 6. Superimposed dislocation rings affect the movement of the dislocation lines in the matrix, when the dislocation lines go through the same position.

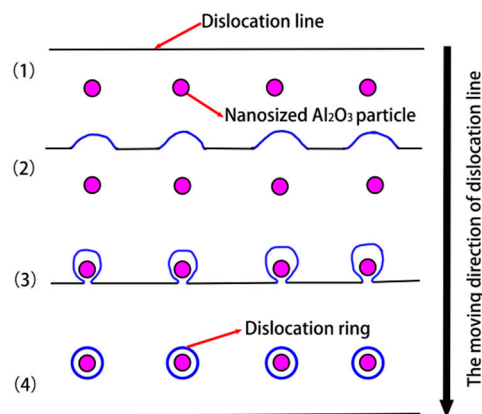


**Figure 6.** The schematic illustration of dislocation through particles mechanism.

Thermal mismatch stress affects the interface between  $\text{Al}_2\text{O}_{3\text{np}}$  particles and  $\alpha\text{-Al}$  in the process of the preparation of composites and the cooling after heat treatment, because the numerical value of the thermal expansion coefficient of the  $\text{Al}_2\text{O}_{3\text{np}}$  particles ( $7.8 \mu\text{m}\cdot\text{mK}^{-1}$ ) is different from that of the 7075 aluminum matrix ( $24.5 \mu\text{m}\cdot\text{mK}^{-1}$ ). New dislocations form due to thermal mismatch stress, and these new dislocations have a dislocation interaction with moving dislocations which reduces dislocation motion and results in the reinforcement of composites [25,26].

Compared to the hardness of  $\text{Al}_2\text{O}_{3\text{np}}/7075$  composites (113.8 HV), the hardness of  $\text{Al}_2\text{O}_{3\text{np}}/7075$  composites under solution treatment (150.4 HV) increased  $\sim 32\%$ . The reason is that the second phase fully dissolved in the matrix after solution treatment, resulting in lattice distortion of the matrix, which leads to solid-solution strengthening. According to the Fleischer formula [27]:

$$\Delta\sigma_{\text{ss}} = MGb\varepsilon_{\text{ss}}^{\frac{3}{2}}\sqrt{c} \quad (2)$$

where,  $\sigma_{\text{ss}}$  represents the yield strength;  $M$  represents the orientation factor;  $G$  represents the shear modulus;  $b$  represents the Burgers vector;  $c$  represents the solute concentration and  $\varepsilon_{\text{ss}}$  represents lattice strain. When Mg, Zn, Cu atoms are alloyed with  $\alpha\text{-Al}$  as solute atoms that differ from the matrix atoms in size, concentration, or shear modulus, which can result in lattice distortion of the composites and cause a variation of strain fields. Strain fields are created that interact with dislocations and impede their motion, leading to an increase in the strength of the composites [28].

Compared to the hardness of  $\text{Al}_2\text{O}_{3\text{np}}/7075$  composites (113.8 HV), the hardness of  $\text{Al}_2\text{O}_{3\text{np}}/7075$  composites under T6 treatment (173.5 HV) increased  $\sim 52\%$ . The reason is that aging precipitation phases interact with dislocations and inhibit dislocation motion. The strengthening mechanism can be divided into two types by the interaction of aging precipitation phases and dislocation lines. The first type is that the dislocation lines cut through the particles when aging precipitation phases are deformable particles. The aging precipitation phases can be divided into two parts by dislocation lines. The two parts of aging precipitation phases glide with the dislocation motion. Therefore, new interfaces between aging precipitation phases and matrix are created, and the total interfacial energy increases. Elastic coherent strain fields are generated around the aging precipitation phases. These strain fields show reciprocal action with moving dislocation lines and inhibit the dislocation motion. The effect of dislocation lines cut through the deformed aging precipitation phases reinforced composites can be expressed as [29]:

$$\Delta\tau = \frac{1.1\gamma_s^{3/2}(r\phi)^{1/2}}{\mu b^2\alpha^{1/2}}, \quad (3)$$

where:  $\gamma_s$  represents the interface energy,  $r$  represents the radius of the aging precipitation phases,  $\phi$  represents the volume fraction of aging precipitation phases,  $\mu$  is the Poisson's ratio,  $b$  is the Burgers

vector, and  $\alpha$  is a constant associated with the shape of the Guinier-Preston (GP) zones, which are clusters that contain a high fraction of solute atoms.

The second type involves the dislocation lines moving around particles and dislocation rings forming around particles when the aging precipitation phases are non-deformable particles. Then, the dislocation lines move again to that position and the superimposed dislocation rings inhibit dislocation motion. The effect of dislocation lines cut through the non-deformable aging precipitation phases reinforced composites can be expressed as [30]:

$$\Delta\tau = \mu br^{-1} \left( \frac{6\phi}{\pi} \right)^{1/3}, \quad (4)$$

In the formula  $r$  represents the radius of the aging precipitation phases,  $\phi$  represents the volume fraction of aging precipitation phases,  $\mu$  is the Poisson's ratio, and  $b$  is the Burgers vector.

The precipitation sequence of  $\text{Al}_2\text{O}_{3\text{np}}/7075$  composites has been reported to be:  $\alpha$ -Supersaturated solid solution  $\rightarrow$  GP Zones  $\rightarrow$   $\eta'$ -Transient phases ( $\text{MgZn}_2$ )  $\rightarrow$   $\eta$ -Equilibrium phases ( $\text{MgZn}_2$ ) [31]. The GP zone phases are easiest to separate because the interface between GP zones phases with the matrix is coherent and the interfacial energy is low. The interfacial energy of  $\eta'$ -Transient phases and  $\eta$ -Equilibrium phases increase, and the degree of coherency decreases [32]. Therefore, separation becomes more difficult.

Compared to the dislocation lines cut through the particles, the strengthening effect of the dislocation lines bypassing particles is better, because dislocation lines need to overcome a larger resistance to bypass the particle [28]. Analysis was conducted in combination with Figure 7a. Figure 7a shows the hardness of  $\text{Al}_2\text{O}_{3\text{np}}/7075$  composites after aging treatments at different temperatures for 24 h. With the extension of aging treatment temperature, the hardness value of  $\text{Al}_2\text{O}_{3\text{np}}/7075$  composites increases first and then decreases. For an time-controlled aging treatment at 24 h, the main aging precipitation phases are GP zones, in addition to a small amount of the  $\eta'$ -Transient phases when the aging treatment temperature is lower. The dislocation motion is mainly cutting through GP zones. Therefore, the strengthening effect is not obvious, and the hardness of the composites is small. With increasing aging treatment temperature, GP zones gradually decrease, and are converted into  $\eta'$ -Transient phases; moreover, the strengthening effect and hardness of composites enhance gradually. The hardness reaches a maximum when the aging treatment happens at 120 °C. And the main aging precipitation phases are  $\eta'$ -Transient phases for an aging treatment temperature of 120 °C. The dislocation motion is mainly bypassing  $\eta'$ -Transient phases, the strengthening effect is best, and the hardness of the composites is largest. The  $\eta'$ -Transient phases grow and coarsen gradually, and transform into stable, large-sized  $\eta$ -Transient phases, resulting in the strengthening of the hardness of composites.

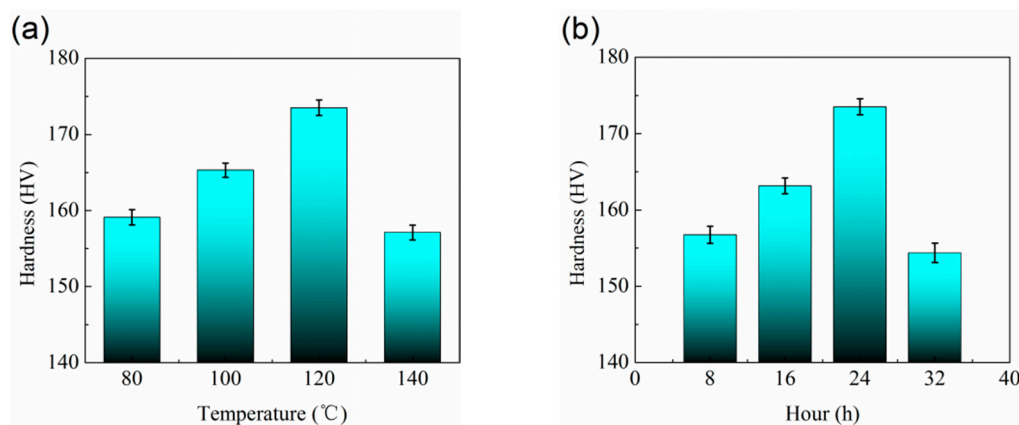


**Figure 7.** (a) Hardness of  $\text{Al}_2\text{O}_{3\text{np}}/7075$  composites aged at different temperature for 24 h; (b) Hardness of  $\text{Al}_2\text{O}_{3\text{np}}/7075$  composites aged at 120 °C for different time.

Analysis was conducted in combination with Figure 7b. Figure 7b shows the hardness of  $\text{Al}_2\text{O}_{3\text{np}}/7075$  composites after aging treatments at  $120^\circ\text{C}$  for different times. With the extension of aging treatment time, the hardness value of  $\text{Al}_2\text{O}_{3\text{np}}/7075$  composites increases first and then decreases. The aging treatment temperature was controlled at  $120^\circ\text{C}$ . With increasing aging treatment time, the GP zones gradually decrease and convert into  $\eta'$ -Transient phases. The hardness of  $\text{Al}_2\text{O}_{3\text{np}}/7075$  composites was higher after 24 h of aging treatment. However, further increasing the aging treatment time leads to decreasing hardness of  $\text{Al}_2\text{O}_{3\text{np}}/7075$  composites. According to the results of the hardness study, it was concluded that the hardness value of  $\text{Al}_2\text{O}_{3\text{np}}/7075$  composites is highest under a solution treatment at  $480^\circ\text{C}$  for 5 h and aging treatment at  $120^\circ\text{C}$  for 24 h. Therefore, the T6 heat treatment condition with solution treatment at  $480^\circ\text{C}$  for 5 h and aging treatment at  $120^\circ\text{C}$  for 24 h is the preferred condition.

#### 4. Conclusions

- (1) The as-cast microstructure of  $\text{Al}_2\text{O}_{3\text{np}}/7075$  composites consists of  $\alpha\text{-Al}$ ,  $\text{Al}_2\text{O}_{3\text{np}}$  particles and eutectic phases  $\text{Mg}(\text{Zn,Cu,Al})_2$  and  $\text{Al}_7\text{Cu}_2\text{Fe}$ .
- (2) In response to solution treatment at  $480^\circ\text{C}$  for 5 h,  $\text{Mg}(\text{Zn,Cu,Al})_2$  phases gradually dissolve into the  $\alpha\text{-Al}$  matrix and a new eutectic phase  $\text{Al}_2\text{CuMg}$  forms. The morphology and size of  $\text{Al}_7\text{Cu}_2\text{Fe}$  phases remain nearly unchanged. After aging treatment, small  $\text{MgZn}_2$  phases separate out.
- (3) The optimum T6 heat treatment situation for  $\text{Al}_2\text{O}_{3\text{np}}/7075$  composites is the solution treatment at  $480^\circ\text{C}$  for 5 h and aging treatment at  $120^\circ\text{C}$  for 24 h.
- (4) Compared to the hardness of 7075 aluminum alloy matrix (94.7 HV), the hardness of  $\text{Al}_2\text{O}_{3\text{np}}/7075$  composites (113.8 HV) increased  $\sim 20\%$ . Compared to the hardness of  $\text{Al}_2\text{O}_{3\text{np}}/7075$  composites (113.8 HV), the hardness of  $\text{Al}_2\text{O}_{3\text{np}}/7075$  composites under solution treatment (150.4 HV) at  $480^\circ\text{C}$  for 5 h increased  $\sim 32\%$  and the hardness of  $\text{Al}_2\text{O}_{3\text{np}}/7075$  composites under optimum T6 heat treatment (173.5 HV) increased  $\sim 52\%$ .

**Author Contributions:** P.-X.Z. and H.Y. conceived and designed the experiments; P.-X.Z. and X.-L.Z. performed the experiments; P.-X.Z., H.Y. and X.-L.Z. analyzed the data; P.-X.Z., H.Y. and B.-B.T. contributed reagents/materials/analysis tools; P.-X.Z., H.Y., W.L., X.-L.Z. and B.-B.T. wrote the paper.

**Funding:** This research was funded by the Natural Science Foundation of Jiangxi Province (20181BAB206026 and 20171BAB206034).

**Conflicts of Interest:** The authors declare no conflict of interest.

#### References

1. Chen, X.H.; Yan, H. Constitutive behavior of  $\text{Al}_2\text{O}_{3\text{np}}/\text{Al}7075$  composites with a high solid fraction for thixoforming. *J. Alloys Compd.* **2017**, *708*, 751–762. [[CrossRef](#)]
2. Alam, S.N.; Kumar, L. Mechanical properties of aluminium based metal matrix composites reinforced with graphite nanoplatelets. *Mater. Sci. Eng. A* **2016**, *667*, 16–32. [[CrossRef](#)]
3. Jiang, J.; Xiao, G.; Che, C.; Wang, Y. Microstructure, mechanical properties and wear behavior of the rheoformed 2024 aluminum matrix composite component reinforced by  $\text{Al}_2\text{O}_3$  nanoparticles. *Metals* **2018**, *8*, 460. [[CrossRef](#)]
4. Xu, H.; Zhang, G.Z.; Cui, W.; Ren, S.B.; Wang, Q.J.; Qu, X.H. Effect of  $\text{Al}_2\text{O}_{3\text{sf}}$  addition on the friction and wear properties of  $(\text{SiC}_p + \text{Al}_2\text{O}_{3\text{sf}})/\text{Al}2024$  composites fabricated by pressure infiltration. *Int. J. Miner. Metall. Mater.* **2018**, *25*, 375–382. [[CrossRef](#)]
5. Qiu, F.; Tong, H.T.; Gao, Y.Y.; Zou, Q.; Dong, B.X.; Li, Q.; Chu, J.G.; Chang, F.; Shu, S.L.; Jiang, Q.C. Microstructures and compressive properties of Al matrix composites reinforced with bimodal hybrid in-situ nano-/micro-sized TiC particles. *Materials* **2018**, *11*, 1284. [[CrossRef](#)] [[PubMed](#)]
6. Carreño-Gallardo, C.; Estrada-Guel, I.; López-Meléndez, C.; Ledezma-Sillas, E.; Castañeda-Balderas, R.; Pérez-Bustamante, R.; Herrera-Ramírez, J.M. B4C particles reinforced Al2024 composites via mechanical milling. *Metals* **2018**, *8*, 647. [[CrossRef](#)]

7. Walczak, M.; Pieniak, D.; Zwierzchowski, M. The tribological characteristics of SiC particle reinforced aluminium composites. *Arch. Civ. Mech. Eng.* **2015**, *15*, 116–123. [[CrossRef](#)]
8. Chen, X.H.; Yan, H.; Jie, J.P. Effects of Ti addition on microstructure and mechanical properties of 7075 alloy. *Int. J. Cast Met. Res.* **2015**, *28*, 151–157. [[CrossRef](#)]
9. Vencel, A.; Bobic, I.; Arostegui, S.; Bobic, B.; Marinković, A.; Babić, M. Structural, mechanical and tribological properties of A356 aluminium alloy reinforced with Al<sub>2</sub>O<sub>3</sub>, SiC and SiC + graphite particles. *J. Alloys Compd.* **2010**, *506*, 631–639. [[CrossRef](#)]
10. Issa, H.K.; Taherizadeh, A.; Maleki, A.; Ghaei, A. Development of an aluminum/amorphous nano-SiO<sub>2</sub> composite using powder metallurgy and hot extrusion processes. *Ceram. Int.* **2017**, *43*, 14582–14592. [[CrossRef](#)]
11. Yang, Y.; Lan, J.; Li, X. Study on bulk aluminum matrix nano-composite fabricated by ultrasonic dispersion of nano-sized SiC particles in molten aluminum alloy. *Mater. Sci. Eng.* **2004**, *380*, 378–383. [[CrossRef](#)]
12. Liu, P.; Wang, A.Q.; Xie, J.P.; Hao, S.M. Effect of heat treatment on microstructure and mechanical properties of SiC<sub>p</sub>/2024 aluminum matrix composite. *J. Wuhan Univ. Technol.* **2015**, *30*, 1229–1233. [[CrossRef](#)]
13. Li, N.; Yan, H.; Wang, Z.W. Effects of heat treatment on the tribological properties of SiC<sub>p</sub>/Al-5Si-1Cu-0.5Mg composite processed by electromagnetic stirring method. *Appl. Sci.* **2018**, *8*, 372. [[CrossRef](#)]
14. Lashgari, H.R.; Zangeneh, S.; Shahmir, H.; Saghafi, M.; Emamy, M. Heat treatment effect on the microstructure, tensile properties and dry sliding wear behavior of A356–10%B<sub>4</sub>C cast composites. *Mater. Des.* **2010**, *39*, 4414–4422. [[CrossRef](#)]
15. Albiter, A.; León, C.A.; Drew, R.A.L.; Bedolla, E. Microstructure and heat-treatment response of Al-2024/TiC composites. *Mater. Sci. Eng. A* **2000**, *289*, 109–115. [[CrossRef](#)]
16. Chen, X.H.; Yan, H. Effect of nanoparticle Al<sub>2</sub>O<sub>3</sub> addition on microstructure and mechanical properties of 7075 alloy. *Int. J. Cast Met. Res.* **2016**, *28*, 337–344. [[CrossRef](#)]
17. Chen, X.H.; Yan, H. Fabrication of nanosized Al<sub>2</sub>O<sub>3</sub> reinforced aluminum matrix composites by subtype multifrequency ultrasonic vibration. *J. Mater. Res.* **2015**, *30*, 2197–2209. [[CrossRef](#)]
18. Liu, C.; Liu, Y.; Ma, L.; Yi, J. Effects of solution treatment on microstructure and high-cycle fatigue properties of 7075 aluminum alloy. *Metals* **2017**, *7*, 193. [[CrossRef](#)]
19. Fan, X.G.; Jiang, D.M.; Meng, Q.C.; Zhong, L. The microstructural evolution of an Al-Zn-Mg-Cu alloy during homogenization. *Mater. Lett.* **2006**, *60*, 1475–1479. [[CrossRef](#)]
20. Zou, X.L.; Yan, H.; Chen, X.H. Evolution of second phases and mechanical properties of 7075 Al alloy processed by solution heat treatment. *Trans. Nonferr. Met. Soc. China* **2017**, *27*, 2146–2155. [[CrossRef](#)]
21. Deng, Y.L.; Wan, L.; Wu, L.H.; Zhang, Y.Y.; Zhang, X.M. Microstructural evolution of Al-Zn-Mg-Cu alloy during homogenization. *J. Mater. Sci.* **2011**, *46*, 875–881. [[CrossRef](#)]
22. Schultz, B.F.; Ferguson, J.B.; Rohatgi, P.K. Microstructure and hardness of Al<sub>2</sub>O<sub>3</sub> nanoparticle reinforced Al-Mg composites fabricated by reactive wetting and stir mixing. *Mater. Sci. Eng. A* **2011**, *530*, 87–97. [[CrossRef](#)]
23. You, G.L.; Ho, N.J.; Kao, P.W. In-situ formation of Al<sub>2</sub>O<sub>3</sub> nanoparticles during friction stir processing of Al/SiO<sub>2</sub> composite. *Mater. Charact.* **2013**, *80*, 1–8. [[CrossRef](#)]
24. Hu, Z.H.; Peng, X.; Wu, G.H.; Cheng, D.Q.; Liu, W.C.; Zhang, L.; Ding, W.J. Microstructure evolution and mechanical properties of rheo-processed ADC12 alloy. *Trans. Nonferr. Met. Soc. China* **2016**, *26*, 3070–3080. [[CrossRef](#)]
25. Sankaranarayanan, S.; Jayalakshmi, S.; Gupta, M. Effect of addition of mutually soluble and insoluble metallic elements on the microstructure, tensile and compressive properties of pure magnesium. *Mater. Sci. Eng. A* **2011**, *530*, 149–160. [[CrossRef](#)]
26. Lei, Z.B.; Zhao, K.; Wang, Y.G.; An, L.N. Thermal expansion of Al matrix composites reinforced with hybrid micro-/nano-sized Al<sub>2</sub>O<sub>3</sub> particles. *J. Mater. Sci. Technol.* **2013**, *40*, 1–4. [[CrossRef](#)]
27. Fleischer, R.L. Substitutional solution hardening durcissement de solution par substitution verfestigung in substitutionsmischkristallen. *Acta Metall. Sin.* **1963**, *11*, 203. [[CrossRef](#)]
28. Ma, K.; Wen, H.; Hu, T.; Topping, T.D.; Isheim, D.; Seidman, D.N.; Lavernia, E.J.; Schoenung, J.M. Mechanical behavior and strengthening mechanisms in ultrafine grain precipitation-strengthened aluminum alloy. *Acta Mater.* **2014**, *62*, 141–155. [[CrossRef](#)]
29. He, Z.J. *Mechanical Properties of Metals*, 1st ed.; Metallurgical Industry Press: Beijing, China, 1989.
30. Orowan, E. *Internal Stresses in Metals and Alloys*, 1st ed.; Institute of Metals: London, UK, 1948.

31. Karabay, S.; Bayraklillar, M.S.; Balci, E. Influence of different heat treatments on the solid particle erosion behavior of aluminum alloy AA7075 in industrial applications. *Acta Phys. Pol. A* **2015**, *127*, 1052–1054. [[CrossRef](#)]
32. Ku, M.H.; Hung, F.Y.; Lui, T.S.; Lai, J.J. Enhanced formability and accelerated precipitation behavior of 7075 Al alloy extruded rod by high temperature aging. *Metals* **2018**, *8*, 648. [[CrossRef](#)]



© 2019 by the authors. Licensee MDPI, Basel, Switzerland. This article is an open access article distributed under the terms and conditions of the Creative Commons Attribution (CC BY) license (<http://creativecommons.org/licenses/by/4.0/>).